Trichloroethene Hydrodechlorination in Water by Highly Disordered Monometallic Nanoiron

Yueqiang Liu,[†] Hyeok Choi,[‡] Dionysios Dionysiou,[‡] and Gregory V. Lowry*[,†]

Department of Civil & Environmental Engineering, Carnegie Mellon University, Pittsburgh, Pennsylvania 15213-3890, and Department of Civil and Environmental Engineering, University of Cincinnati, Cincinnati, Ohio 45221-0071

Received May 26, 2005. Revised Manuscript Received August 1, 2005

The small size and high surface-to-volume ratio makes nanoiron attractive for in situ remediation of groundwater contaminants that are susceptible to reductive transformation, e.g. trichloroethylene (TCE). Nanoiron synthesized from borohydride reduction of dissolved iron is the most widely studied. Its reactivity with chlorinated organics such as trichloroethylene (TCE) is unique compared to other nanoiron and to iron filings that are typically used for in situ groundwater remediation, e.g. (1) higher surface-area normalized TCE dechlorination reaction rate constants, (2) the formation of saturated reaction products, and (3) higher reaction rates in the presence of H_2. The objectives of this study were to confirm the ability of monometallic Fe(B) to activate and use H_2 for TCE hydrodechlorination and to determine how the nanoiron chemical composition and the degree of crystallinity influence nanoiron reactivity with TCE. Fresh (Fe(B)), partially oxidized ($Fe(B)^{ox}$), and annealed ($Fe(B)^{cr}$) nanoiron samples made from borohydride reduction of dissolved Fe(II) in a water/methanol solution were characterized by HRTEM, XRD, XPS, and N_2-BET. The TCE dechlorination rate and products and the dissolved iron and boron released during reaction with TCE were measured. Fe(B) and $Fe(B)^{ox}$ were poorly ordered and could activate and use H_2 to reduce TCE to ethane. $Fe(B)^{cr}$ was crystalline and could not activate and use H_2 and reduced TCE to acetylene. The poorly ordered structure rather than the presence of boron (up to 5 wt %) provided the ability of Fe(B) and $Fe(B)^{ox}$ to activate and use H_2 for TCE dechlorination. Fe(B) and $Fe(B)^{ox}$ underwent oxidative dissolution during TCE dechlorination, and the Fe^0 in the particles was fully accessible. Particle dissolution suggests that normalizing the observed reaction rate constants with the measured specific surface area for comparison with other types of Fe^0 may be inappropriate.

Introduction

The use of nanoiron for in situ remediation of groundwater contaminants is promising. The small size and high reactivity of nanoiron compared with micrometer-sized iron filings makes them attractive for in situ application, e.g. injection into the subsurface to dechlorinate chlorinated organics such as trichloroethylene (TCE). The high reactivity of nanoiron has been attributed to their large specific surface area.[1−3] The expanding list of contaminants that are rapidly reduced by nanoiron or bimetallic nanoparticles now includes chlorinated organics,[1−11] heavy metals,[12−14] inorganic anions,[15−17] and other contaminants.[7,11,14,18]

In the absence of reductants other than Fe^0, iron oxidation by TCE can be described by the half-reactions eqs 1 and 2, where the values of x and y depend on the products formed.[10,19,20] Water can also oxidize Fe^0 resulting in H_2 and OH^-(aq) (eq 3). These reactions are thermodynamically favorable[13,21] (standard potentials are adjusted to pH = 7 and 1 mM Cl^-).

* Corresponding author. E-mail: glowry@cmu.edu.
[†] Carnegie Mellon University.
[‡] University of Cincinnati.

(1) Wang, C. B.; Zhang, W. X. *Environ. Sci. Technol.* **1997**, *31*, 2154−2156.
(2) Lien, H. L.; Zhang, W. X. *J. Environ. Eng. (Reston, Va.)* **1999**, *125*, 1042−1047.
(3) Schrick, B.; Blough, J. L.; Jones, A. D.; Mallouk, T. E. *Chem. Mater.* **2002**, *14*, 5140−5147.
(4) Zhang, W.-x.; Wang, C.-B.; Lien, H.-L. *Catal. Today* **1998**, *40*.
(5) Elliott, D. W.; Zhang, W. *Environ. Sci. Technol.* **2001**, *35*, 4922−4926.
(6) Lien, H. L.; Zhang, W. X. *Colloids Surf., A* **2001**, *191*, 97−105.
(7) Zhang, W. *J. Nanopart. Res.* **2003**, *5*, 323−332.
(8) Lowry, G. V.; Johnson, K. M. *Environ. Sci. Technol.* **2004**, *38*, 5208−5216.
(9) Quinn, J.; Geiger, C.; Clausen, C.; Brooks, K.; Coon, C.; O'Hara, S.; Krug, T.; Major, D.; Yoon, W.-S.; Gavaskar, A.; Holdsworth, T. *Environ. Sci. Technol.* **2005**, *39*, 1309−1318.
(10) Liu, Y.; Majetich, S. A.; Tilton, R. D.; Sholl, D. S.; Lowry, G. V. *Environ. Sci. Technol.* **2005**, *39*, 1338−1345.
(11) Nurmi, J. T.; Tratnyek, P. G.; Sarathy, V.; Baer, D. R.; Amonette, J. E.; Pecher, K.; Wang, C.; Linehan, J. C.; Matson, D. W.; Penn, R. L.; Driessen, M. D. *Environ. Sci. Technol.* **2005**, *39*, 1221−1230.
(12) Ponder, S. M.; Darab, J. G.; Mallouk, T. E. *Environ. Sci. Technol.* **2000**, *34*, 2564−2569.
(13) Ponder, S. M.; Darab, J. G.; Bucher, J.; Caulder, D.; Craig, I.; Davis, L.; Edelstein, N.; Lukens, W.; Nitsche, H.; Rao, L.; Shuh, D. K.; Mallouk, T. E. *Chem. Mater.* **2001**, *13*, 479−486.
(14) Shimotori, T.; Nuxoll, E. E.; Cussler, E. L.; Arnold, W. A. *Environ. Sci. Technol.* **2004**, *38*, 2264.
(15) Choe, S.; Chang, Y.-Y.; Hwang, K.-Y.; Khim, J. *Chemosphere* **2000**, *41*, 1307−1311.
(16) Mondal, K.; Jegadeesan, G.; Lalvani, S. B. *Ind. Eng. Chem. Res.* **2004**, *43*, 4922−4934.
(17) Kanel, S. R.; Manning, B.; Charlet, L.; Choi, H. *Environ. Sci. Technol.* **2005**, *39*, 1291−1298.
(18) Joo, S. H.; Feitz, A. J.; Sedlak, D. L.; Waite, T. D. *Environ. Sci. Technol.* **2005**, *39*, 1263−1268.
(19) Gillham, R. W.; F., O. H. S. *Groundwater* **1994**, *32*, 958−967.
(20) Orth, W. S.; Gillham, R. W. *Environ. Sci. Technol.* **1996**, *30*, 66−71.

10.1021/cm0511217 CCC: $30.25
Published on Web 09/28/2005

$$Fe^0 \rightarrow Fe^{2+} + 2e^- \quad E_H{}^0 = +0.447\ V \qquad (1)$$

$$TCE + xH^+ + ye^- \rightarrow prod + (y-x)Cl^- \quad E_{H,c,t,1,1-DCE}{}^0 = +0.52 \pm 0.02\ V \qquad (2)$$

$$2H_2O + 2e^- \rightarrow H_2 + 2OH(aq)^- \quad E_H{}^0 = -0.379\ V \qquad (3)$$

Because TCE dechlorination is the desired reaction, the competing reaction with water is undesirable. Water as a competing oxidant is less important if the H_2 formed (eq 3) can be activated and used to dechlorinate TCE via hydrodechlorination (eq 4).

$$H_2(g) \leftrightarrow 2H_{ad} \leftrightarrow 2H(aq)^+ + 2e^- \quad E_H{}^0 = +0.379\ V \qquad (4)$$

The dissociative adsorption (activation) of $H_2(g)$ by noble metals (e.g. Pd, Pt, Rh) is widely reported and commonly exploited in the chemical industry,[22] and palladium-catalyzed hydrodechlorination of TCE by $H_2(aq)$ in water has been reported.[23] Dissociative hydrogen adsorption (activation) onto monometallic nanoiron has not been reported; however, it is not unprecedented. For example, dissociative adsorption of $H_2(g)$ onto pure iron surfaces in the gas phase has been reported.[24] The use of iron as hydrogenation catalysts (Fischer−Tropsch) is also common but typically uses high temperatures (475 K) and pressures (15−20 bar).[25]

TCE dechlorination to partially or fully dechlorinated products proceeds using Fe^0 as the reductant (eq 5) or using H_2 as the reductant (eq 6).

The values of the coefficients a and b are determined by the products formed, e.g. $a = 4$ and $b = 3$ for ethane and $a = 2$ and $b = 3$ for acetylene. The ability of nanoiron to activate and use H_2 for the hydrodechlorination of TCE will increase the efficiency of the nanoiron because electrons used to reduce water to H_2 can then be used to reduce TCE rather than lost.

$$aFe^0 + TCE + (2a-b)H^+ \rightarrow prod + aFe^{2+} + bCl^- \qquad (5)$$

$$aH_2 + TCE \rightarrow prod + bH^+ + bCl^- \qquad (6)$$

Nanoiron synthesized from the borohydride ($BH_4^-(aq)$) reduction of dissolved Fe(II) or Fe(III) is the most studied nanoiron to date.[1−18] For example, borohydride reduction has been used to synthesize reactive "ferrogels" for reduction of heavy metals in water,[13] to synthesize bimetallic (Ni−Fe, Pd−Fe) nanoparticles for trichloroethylene reduction in water,[1,3] and to synthesize carbon and polymer-supported nanoiron designed to be mobile in the environment.[26] It is often reported that these particles are α-Fe^0, and reactivity comparisons with micrometer-sized granular iron filings are commonly invoked.[1−3,6−8] Freshly synthesized nanoiron has been characterized,[1,3,13] and in a few cases the nanoiron has been characterized after exposure to heavy metals or chlorinated organic contaminants in water to determine the coprecipitated heavy metals on the particle surface[12] or to observe changes in the particle properties as a result of the reaction.[11] Most nanoiron studies have focused on contaminant degradation kinetics and the reaction products, however, and less is known about the physical and chemical changes occurring to the nanoiron during reaction and how these changes affect nanoiron reactivity.

Table 1. Differences between Fe(B) and RNIP[10]

param	Fe(B)	RNIP
primary particle size (nm)	20−40	40−60
BET SA (m^2/g)	36	23
crystallinity	highly disordered	crystalline
B content (wt %, bulk) (at. %)	5 (18)	0
TCE reacn order	zero-order	first-order
reacn rate constant	2×10^{-3} mmol·h^{-1}·m^{-2}	4×10^{-4} L·h^{-1}·m^{-2}
products	saturated	unsaturated
able to activate H_2	yes	no

The reduction reactions promoted by zerovalent iron are surface mediated, so their reactivity is primarily controlled by their near surface composition.[27−29] For nanoiron, the high surface-to-volume ratio makes it difficult to distinguish the near surface from the bulk, and significant changes in nanoiron morphology and Fe^0 content may occur in a short time (days) that affects their reactivity. For example, the PCB dechlorination rate afforded by nanoiron synthesized by borohydride reduction was 1 order of magnitude lower for particles that had been exposed to air than for fresh particles, presumably due to formation of a surface metal oxide layer.[8] Nanoiron synthesized by the gas-phase reduction of Fe−oxides[30] (RNIP) afforded very different TCE dechlorination rates and products than for nanoiron synthesized from borohydride reduction (Fe(B)), despite having similar physical properties (e.g. primary particle size and specific surface area[10]). This suggests that nanoiron physical and chemical properties other than particle size and surface area strongly affect their reactivity. A summary of the differences between these particle types is provided in Table 1. Important differences are that Fe(B) appeared to be able to activate and use H_2 produced from the reduction of water to hydrodechlorinate TCE and that the products of TCE reduction with Fe(B) were primarily saturated (e.g. ethane). RNIP could not activate or use H_2 and yielded primarily unsaturated products (e.g. acetylene).

There are several possible reasons for the unique reactivity of Fe(B) compared to RNIP and to iron filings. These include differences in the chemical composition of the surface, the

(21) Vogel, T. M.; Criddle, C. S.; McCarty, P. L. *Environ. Sci. Technol.* **1987**, *21*, 722−736.
(22) Mitsui, T.; Rose, M. K.; Fomin, E.; Ogletree, D. F.; Salmeron, M. *Nature* **2003**, *422*, 705−707.
(23) Lowry, G. V.; Reinhard, M. *Environ. Sci. Technol.* **1999**, *33*, 1905−1910.
(24) Paal, Z.; Menon, P. G. *Hydrogen effects in Catalysis: fundamentals and practical applications*; M. Dekker: New York, 1988.
(25) Pyatnitskii, Y. I.; Chashechnikova, I. T.; Pavlenko, N. V. *Theor. Exp. Chem.* **1996**, *32*, 103−107.
(26) Schrick, B.; Hydutsky, B. W.; Blough, J. L.; Mallouk, T. E. *Chem. Mater.* **2004** *16* (11), 2187−2193.
(27) Gaspar, D. J.; Lea, A. S.; Engelhard, M. H.; Baer, D. R. *Langmuir* **2002**, *18*, 7688−7693.
(28) Klausen, J.; Vikesland, P. J.; Kohn, T.; Burris, D. R.; Ball, W. P.; Roberts, A. L. *Environ. Sci. Technol.* **2003**, *37*, 1208−1218.
(29) Kohn, T.; Livi, K. J. T.; Roberts, A. L.; Vikesland, P. J. *Environ. Sci. Technol.* **2005**, *39* (8), 2867−2879.
(30) Uegami, M.; Kawano, J.; Okita, T.; Fujii, Y.; Okinaka, K.; Kakuya, K.; Yatagai, S. Iron particles for purifying contaminated soil or groundwater, process for producing the iron particles, purifying agent comprising the iron particles, process for producing the purifying agent and method of purifying contaminated soil or groundwater. U.S. 20030217974A1, 2003.

degree of crystallinity of the particles, and the presence of boron. The highly disordered structure of Fe(B)[31−33] and the crystalline nature of RNIP[10,11] have been reported. Highly disordered zerovalent metals may react differently from their crystalline analogues due to weaker atomic interactions and a higher number of structural defects than in crystalline solids. For example, Yokoyama et al. demonstrated that amorphous ribbons of metal−B alloy were more reactive than crystalline ribbons with the same composition in the catalytic hydrogenation of CO.[34] It has also been speculated that boron may be responsible for the unique reactivity as boron is present at ∼18 at. % in Fe(B) but not detected in RNIP.[3,10,11,13]

The objectives of this study are to confirm the ability of monometallic Fe(B) to activate and use H_2 for TCE hydrodechlorination and to determine how the nanoiron chemical composition and the degree of crystallinity influence nanoiron reactivity with TCE. Nanoiron was synthesized by borohydride reduction of dissolved Fe(II) in a water methanol mixture as previously described.[10] The nanoiron properties were altered by exposing them to air to partially oxidize them or annealed in H_2 at 400 °C to crystallize them. The physical and chemical properties of fresh, partially oxidized, and annealed particles were determined using high-resolution transmission electron microscopy (HRTEM), selected area electron diffraction (SAED), X-ray diffraction (XRD), X-ray photoelectron spectroscopy (XPS), and N_2-BET specific surface area. To investigate the effect of partial oxidation and the degree of crystallinity on nanoiron reactivity and how these properties affect the ability to activate and use H_2, the TCE dechlorination rates and product distributions were measured for each particle type in batch reactors in an argon headspace and in a H_2 headspace. To monitor changes in the chemical composition of the nanoiron during reaction, the release of iron and boron into solution was measured during reaction with TCE. The differences in reactivity between fresh, oxidized, and annealed particles were correlated with their measured properties.

Experimental Section

Chemicals. Ferrous sulfate ($FeSO_4 \cdot 7H_2O$) (99.7%), sodium borohydride ($NaBH_4$) (98+%), concentrated HCl (37%), AA iron standard (1000 ppm), and $Na_3B_4O_7 \cdot 10H_2O$ (99+%) were supplied by Fisher Scientific. TCE (99.5+%), *cis*-1,2-dichloroethylene (*c*-DCE) (98%), *trans*-1,2-dichloroethylene (*t*-DCE) (98%), and 1,1-dichloroethylene (1,1-DCE) (99%) were purchased from Aldrich. Methanol (histological grade) was purchased from Acros. Olefin standards (1000 ppm of ethylene, propene, butene, pentene, hexene), paraffin standards (1020 ppm of methane, ethane, propane, butane, pentane, hexane), acetylene (1000 ppm, 1%), ethylene (1%), ethane (1%), vinyl chloride (VC) (10 ppm), and hydrogen (1.08%) were obtained from Alltech. The balance of each was N_2, and all reported concentrations are ±2% of the reported concentration. Ultra high purity argon, hydrogen (5.18%), and compressed N_2 were purchased from Butler Gas products (Pittsburgh, PA).

Particle Synthesis and Preparation. Fe(B) particles were prepared by aqueous phase reduction of dissolved ferrous sulfate using an excess of sodium borohydride as previously described.[10] Particles synthesized for this study, however, were thoroughly rinsed in methanol five times to remove excess salts in the reaction mixture prior to drying. To investigate the effect of air exposure on particle reactivity, some iron particles were exposed to air for ∼3 days at ambient temperature ($Fe(B)^{ox}$) prior to characterization and reactivity studies. To investigate how the degree of crystallinity affects particle reactivity, some particles were annealed at 400 °C in H_2 (99+%) for 3 h ($Fe(B)^{cr}$) before characterization and reactivity studies. The fresh and the derivative particles were stored in an anaerobic glovebox (Ar) prior to use.

Iron Characterization. The nanoiron particle size and morphology was determined using a JEM-2010F HRTEM with SAED. Particles were dispersed (sonicated) in hexane or toluene and then dripped onto a 300 mesh Cu TEM grid coated with Formvar or lacey carbon. The N_2 BET-specific surface area and porosity of the particles were measured using a Tristar 3000 (Micromeritics) BET-surface area analyzer. A Rigaku Geigerflex XRD with a Cu Kα X-ray source (35 kV and 25 mA) was used to determine the phases present and to qualitatively assess the degree of crystallinity of the particles. For each scan, 2θ was increased from 10.0 to 80.0 deg with a step of 0.05 and counting time of 2.0 s. Fe^0 and oxide phases were identified by matching at least two diffraction peaks from 2θ 10−80° using Philips X′pert Graphics and Identity. The particle surface chemical composition was determined using XPS (Perkin-Elmer model 5300) with Mg Kα X-rays at a step size of 0.5 eV for the survey spectrum and 0.05 eV for the high-resolution spectrum.

The Fe^0 content (fresh and reacted particles) was determined by digesting the particles in 1 M HCl and measuring the H_2(g) evolved as described in ref 10. After acid digestion, the total Fe content and B content of the particles was also measured. Total dissolved iron was measured using a GBC 908 flame atomic absorption spectrometer (AAS, $\lambda = 248.3$ nm). The method had ±10% error between replicates and a detection limit of 1 $mg \cdot L^{-1}$. Total dissolved boron was determined using a colorimetric (carmine) method according to American Water Works Association (AWWA) standard method 4500-B/C for concentrations <10 mg/L. The method has ±0.6% error between replicates and a detection limit of 0.02 mg/L.

Batch Reactions. Batch experiments were conducted in 160 mL serum bottles capped by Teflon Mininert valves. The reactors were prepared either in an anaerobic glovebox (argon) or in a H_2-filled glovebag depending on the desired initial conditions, i.e., Ar headspace or H_2 headspace. Each contained 100 mL of deoxygenated water, 60 mL of headspace, and a specified mass of nanoiron and TCE. Pure phase TCE was added to provide the desired initial TCE concentration. The reactors were rotated on an end-over-end rotator at 30 rpm at 22 ± 1 °C. All reactions were evaluated under iron-limited conditions using a low iron to TCE ratio [TCE (∼2.2 mM):Fe^0 (6.3 mM for Fe(B) and $Fe(B)^{cr}$, 2.7 mM for $Fe(B)^{ox}$)]. Dechlorination of TCE to ethane requires 4 mol of Fe^0 (8 mol of electrons)/mol of TCE. Iron-limited conditions (i.e. excess TCE) ensure that all of the Fe^0 would be consumed if it were accessible. Reactions were conducted using an argon headspace or a pure H_2 headspace. In control experiments without nanoiron, it was demonstrated that other TCE loss mechanisms (e.g. photodegradation, adsorption, leakage) were negligible. Mass transfer resistance at the vapor/liquid interface was not considered as these phases are assumed to be in equilibrium.

(31) Wonterghem, J. v.; Morup, S.; Koch, C. J. W.; Charles, S. W.; Wells, S. *Nature* **1986**, *322*, 622−623.
(32) Shen, J.; Li, Z.; Yan, Q.; Chen, Y. *J. Phys. Chem.* **1993**, *97*, 8504−8511.
(33) Hu, Z.; Fan, Y.; Wu, Y.; Yan, Q.; Chen, Y. *J. Mater. Sci.* **1996**, *31*, 611−616.
(34) Yokoyama, A.; Komiyama, H.; Inoue, H. *J. Catal.* **1981**, *68*, 355−361.

Table 2. Characterization of Fe(B), Fe(B)^{ox}, and Fe(B)^{cr}

param	Fe(B)	Fe(B)^{ox}	Fe(B)^{cr}
size (nm)	25−40	25−40	25−40
BET SA (m^2/g)	33.7	19.7	16.9
shell thickness (nm)	5−6	4−5	2.5−4
shell composn by XPS (at. %)	B: 5	B: 8	B: 23
	Fe: 17	Fe: 15	Fe: 4
	O: 53	O: 53	O: 50
crystallinity	highly disordered	highly disordered	crystalline
tot. Fe content (wt %)	89	73	90
Fe^0 content (wt %, bulk)	86	38	89
B content (wt %, bulk) (at. %[a])	5.2 (20)	4.0 (15)	5.1 (20)

[a] Atomic percent was calculated by assuming the balance of total iron and boron is oxygen.

The TCE transformation rates of Fe(B)^{cr} were evaluated using a kinetic modeling software package, Scientist, v. 2.01 (Micromath, St. Louis, MO). The loss of TCE and formation of products were fit concurrently. Reaction pathways for RNIP proposed by Liu et al.[10] were used for Fe(B)^{cr}. Errors reported with reaction rate constants are 95% confidence intervals for the data fits. The reaction kinetics for Fe(B) and Fe(B)^{ox} are more complex than for Fe(B)^{cr} because H_2 is both generated and used during the reaction so rigorous kinetic models of TCE dechlorination by these particles were not developed. Kinetic models for these particles are under further investigation and are not critical for interpreting the data from this study.

Analytical Methods. A 100 μL headspace sample was withdrawn from reactors and analyzed for TCE and its products using a 30 m GSQ PLOT capillary column on a HP 6890 GC/FID. Complete details of the analytical procedure including detection limits were reported previously.[23] A 100 μL headspace sample was also analyzed for H_2 using GC/TCD as described by Liu et al.[10] with a detection limit of 10 μmol·L^{-1}. A relative error of ±2% was determined among the 5 replicate samples.

To quantify dissolved Fe and B, a 1.5- or 2-mL aliquot of the reaction solution was removed for analysis. An equivalent amount of argon gas was injected at each sampling to compensate for the volume change and avoided introducing air into the reactor. The solution was filtered through a 20-nm syringe filter (Whatman) to remove any particles. Total dissolved iron was measured using AAS as described above; total dissolved boron was determined using the colorimetric (carmine) method as described above.

Nanoiron particles recovered after reaction were washed >3 times with acetone and vacuum-dried under argon. Dried particles were then analyzed by HRTEM to determine their morphology. The Fe^0 and boron content of recovered particles was also determined after acid digestion.

Results and Discussion

Particle Characterization. The measured physical and chemical properties of Fe(B), Fe(B)^{ox}, and Fe(B)^{cr} are summarized in Table 2. HRTEM and SAED images of representative particles are shown in Figure 1. XRD patterns collected for Fe(B), Fe(B)^{ox}, and Fe(B)^{cr} are shown in Figure 2.

Fe(B). The HRTEM image (Figure 1a) shows the spherical shape of Fe(B) particles with a primary size of 25−40 nm. The particles are 86 wt % Fe^0 and 5 wt % boron. The balance is assumed to be oxygen present as amorphous Fe−oxide or B−oxide. The N_2-BET specific surface area is 33.7 m^2/g, and the particles are essentially nonporous (0.2 cm^3/g pore volume). The measured particle properties are consistent with previous reports even though the particles were synthesized using slightly different conditions (i.e. adding $NaBH_4$ as a solution rather than powder and oven-drying at 105 °C rather than vacuum-drying).[3,11] The particles appear to have a core/shell structure with a shell thickness of 5−6 nm, consistent with other reports in the literature.[11,35] A clear contrast between the core and the shell is evident, suggesting a denser (higher *Z*-value) material in the core compared to the shell.

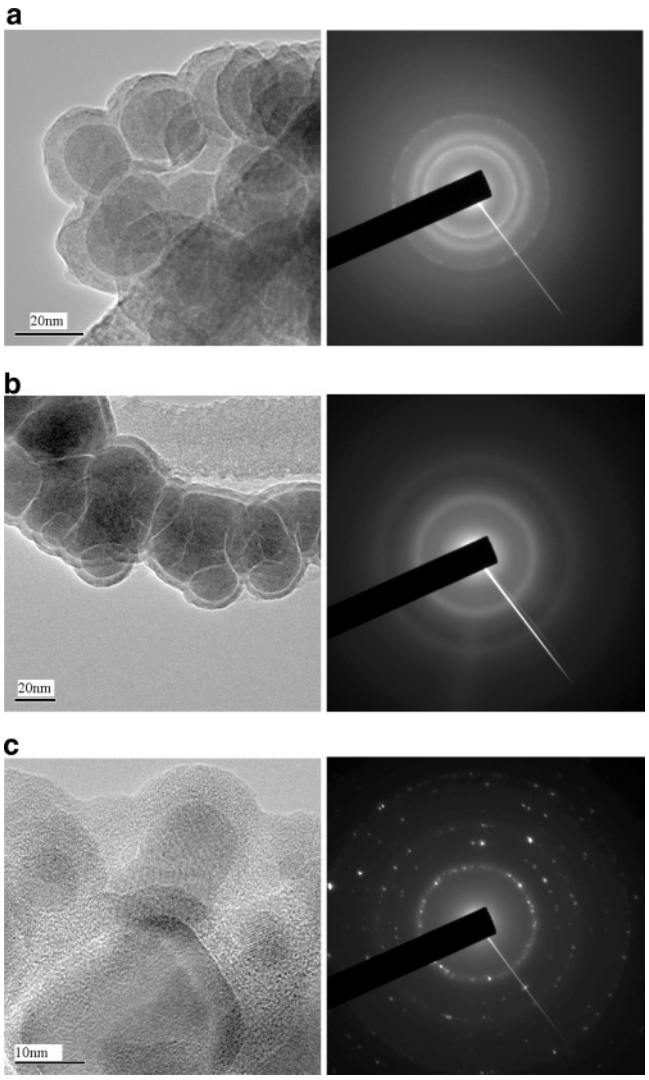

Figure 1. HRTEM images and SAED of nanoiron before reaction: (a) Fe(B); (b) Fe(B)^{ox}; (c) Fe(B)^{cr}.

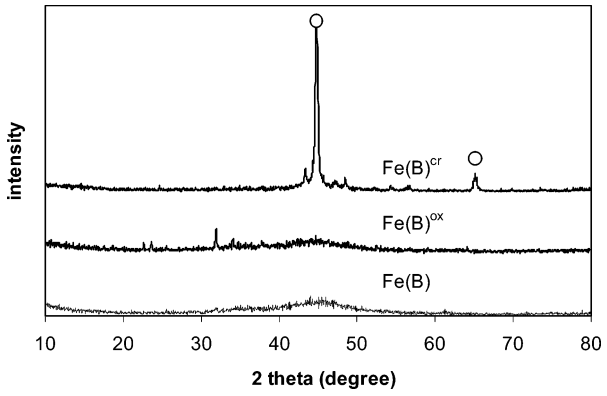

Figure 2. XRD patterns: (a) Fe(B); (b) Fe(B)^{ox}; (c) Fe(B)^{cr} (O: α-Fe^0).

(35) Pankhurst, Q. A.; Martinez, A. Y.; Barquin, L. F. *Phys. Rev. B* **2004**, *69*, 212401.

Table 3. Final TCE Reaction Products from Fe(B), Fe(B)^{ox}, and Fe(B)^{cr}

headspace		Fe(B) (%)[a]		Fe(B)^{ox} (%)		Fe(B)^{cr} (%)	
		Ar	H_2	Ar	H_2	Ar	H_2
1-C	methane	trace[c]	trace	0.7	0.7	trace	trace
2-C	ethene	trace	trace	3.0	1.3	11	13
	ethane	64	77	62	72	trace	trace
	acetylene	ND	ND	ND	ND	83	81
3-C	propylene	1.9	trace	2.9	0.7	trace	0.5
	propane	2.5	2.1	1.4	1.9	trace	trace
4-C	butene	6.8	3.9	10.2	5.3	1.9	1.9
	butane	9.8	9.2	6.0	9.5	1.0	0.8
5-C	5-carbons	4.3	1.8	4.6	2.3	1.1	0.8
6-C	6-carbons	8.6	4.9	9.2	5.7	1.7	0.8
CP[b]	VC	ND[d]	ND	0.03	0.02	0.01	0.02
	c-DCE	0.2	0.06	1.8	0.18	1.4	1.6

[a] Percent of TCE transformed (e.g. 2 mol of TCE = 1 mol of C_4H_{10}). [b] CP = chlorinated products. [c] Trace indicates percentage less than 0.5% for hydrocarbons except for CP. [d] ND = not detected.

The absence of lattice fringes and the diffuse rings observed with SAED indicate that they are poorly ordered or amorphous. This is further confirmed by a broad XRD peak centered at 45° 2θ (Figure 2). Using the Scherrer equation, the peak width at half-maximum corresponds to a crystallite grain size of ~1.0 nm, consistent with Nurmi et al.[11] This grain size indicates a short-range order structure considering that the unit cell dimension of the bcc α-Fe is ~0.29 nm (i.e. 3−4 unit cells/1 nm of crystallite). At this scale, the distinction between amorphous and polycrystalline becomes ambiguous. Broad XRD peaks at 45° 2θ expected for α-Fe^0 have been reported for these particles,[8,10,31,35] but the poorly ordered nature of the particles is a structural feature rarely considered in interpreting nanoiron reactivity data. The high degree of disorder of these particles and the abundant defects originated in the short-range order structure gives them their unique reactivity with TCE that is described below.

Fe(B)^{ox}. For partially oxidized particles, the Fe^0 and B content are 38 and 4 wt %, respectively, and the BET surface area is 19.7 m^2/g. No significant differences were observed between Fe(B)^{ox} and Fe(B) using HRTEM (Figure 1) even though the Fe^0, total iron, and total B content for the partially oxidized particles are lower than for Fe(B) due to the partial oxidation of Fe^0 and a ~25 wt % gain of mass. The mass gain is presumably due to oxygen addition as Fe−oxide or Fe−B−oxides. The oxides formed are poorly ordered or amorphous, however, because no peaks for Fe−oxides were detected using XRD. The surface composition (XPS) was also not significantly different than for fresh particles indicating that the near-surface chemical composition is relatively unaffected by exposure to air. Despite the oxidation of ~50% of the Fe^0 in the particles, the thickness of the TCE-observable shell is unchanged relative to that for fresh particles. The consistent thickness of the HRTEM-observable shell and the unchanged chemical composition of the surface indicate that the shell may be an artifact of the borohydride synthesis method and is likely to be B−oxide or mixed Fe−B−oxide as suggested by Nurmi et al.[11]

Fe(B)^{cr}. The Fe(B)^{cr} particles are 20−40 nm diameter primary particles with an apparent core/shell structure (Figure 1c). The TEM-observable shell is still 3−4 nm thick and lacks lattice fringes and, therefore, poorly ordered or amorphous. A significant enrichment in B (and concomitant decrease of Fe) at the surface of the Fe(B)^{cr} relative to Fe(B) and Fe(B)^{ox} was observed. The core, which showed lattice fringes and a higher TEM contrast than the shell, is crystalline α-Fe^0 as this was the only phase identified with XRD. The clear spots and sharp rings on the SAED patterns and sharpness of its peaks on XRD confirm the crystallinity of the particles (Figure 2). Annealing at high temperatures is a well-known technique to increase the crystallinity of poorly ordered materials.[31,33,36,37] The increased concentration of boron in the particle shell is also a result of the annealing. Boron is "squeezed out" to the exterior of the particles upon crystallization of the core.[33,36,37] The N_2-BET specific surface area is 16.9 m^2/g and lower than for Fe(B) but similar to Fe(B)^{ox}.

TCE Dechlorination. The TCE dechlorination rate, product distribution, and ability to activate and use externally supplied H_2(g) for TCE dechlorination was evaluated in batch reactors for Fe(B), Fe(B)^{ox}, and Fe(B)^{cr}. The sum of the reaction products (Table 3) formed per mole of Fe^0 added to the reactor is shown in Figure 3. The theoretical values included in Figure 3 represent the moles of TCE dechlorination products that could be formed per mole of Fe^0 supplied if all the Fe^0 added were accessible and no other reductants are present. It assumes 2 electrons/mol of Fe^0 are available and is based on the final composition of the products; e.g. 7.6 mol of electrons is needed to transform 1 mol of TCE into 1 mol of the observed products for Fe(B) (mostly ethane). On the basis of the products formed, the theoretical values for Fe(B), Fe(B)^{ox}, and Fe(B)^{cr} are 0.26, 0.27, and 0.46 mol of products/mol of Fe^0, respectively. Because H_2 was both generated (eq 3) and consumed (eq 6) during the reactions, the headspace H_2 concentration in each reactor was also monitored over time (Figure 4). The dissolution of Fe and B from the particles during the reaction with TCE is shown in Figure 5.

Fe(B) (Baseline). The TCE reaction kinetics are complex and cannot be described using pseudo-first-order kinetics. Product formation showed a clear lag phase (~10 h of slow reaction), followed by 2−3 days of steady rapid reaction, and finally a period where the reaction slows and eventually stops (Figure 3a, filled symbols). TCE was transformed

(36) Sanchez, F. H.; Zhang, Y. D.; Budnick, J. I. *Phys. Rev. B* **1988**, *38*, 8508−8510.
(37) Zhang, Y.; Czubayko, U.; Wanderka, N.; Naundorf, V.; Zhu, F.; Wollenberger, H. *Scr. Mater.* **2001**, *44*, 263−267.

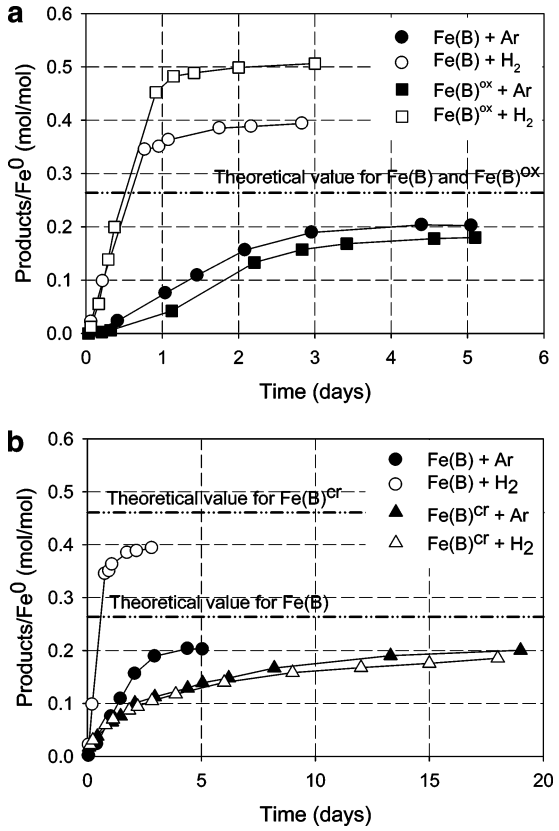

Figure 3. Total TCE reaction products formed in batch reactors: (a) Fe(B) and Fe(B)^{ox}; (b) Fe(B) and Fe(B)^{cr}. All reactors contained a total of 40 mg of iron particles (Fe^0 concentration: 6.3 mM for Fe(B) and Fe(B)^{cr}; 2.7 mM for Fe(B)^{ox}) and 2.2 mM TCE.

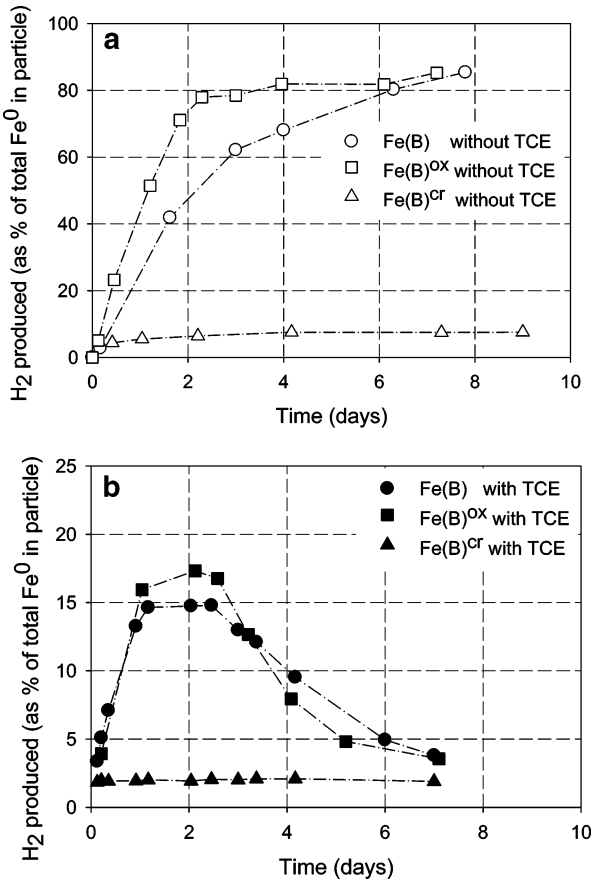

Figure 4. H_2 concentration in the headspace for Fe(B), Fe(B)^{ox}, and Fe(B)^{cr} reactions in Ar: (a) 20 mg of particles without TCE; (b) 40 mg of particles with 2.2 mM TCE.

primarily to nonchlorinated mostly saturated hydrocarbons, 62−64% ethane and ∼36% of coupling products (Table 3). Ethene was a reactive intermediate and finally reduced to ethane. Only small amounts of chlorinated products (VC, <0.3%; *c*-DCE, <2%) were observed.

H_2 Evolution and Utilization and Its Effect on TCE Reactivity. Without TCE present, more than 80% of the Fe^0 in Fe(B) corrodes to produce H_2 after 7 days (Figure 4a), indicating that all of the Fe^0 in Fe(B) is accessible and available for reaction. With TCE present, H_2 is evolved (eq 3) and subsequently utilized in the reaction with TCE (Figure 4b). Approximately 16 wt % of the Fe^0 present in the particles could be accounted for as H_2 (based on an electron balance) during the period of steady reaction ($t = 1-3$ days), but H_2 accounts for less than 4 wt % of the Fe^0 when TCE dechlorination stopped. Adding H_2 to the reactor headspace prior to reaction shortened the lag phase (<2 h), and reactions were ∼4-fold faster than in argon and 90% complete after 1 day (Figure 3a, open symbols). In H_2, the amount of saturated reaction products also increases compared to Ar with ethane accounting for 77% of the products (Table 3). Approximately 20% of the H_2 in the headspace was consumed and used to dechlorinate TCE (data not shown). The facts that more TCE reduction products were produced than theoretically feasible based on the electrons available from Fe^0 alone (Figure 3a, open symbols) and that H_2 was both produced and consumed during reaction with TCE (Figure 4b) are conclusive lines of evidence demonstrating the ability of Fe(B) to activate and utilize H_2. The higher fraction of saturated products in the presence of H_2 is further evidence of the ability of poorly ordered Fe(B) to activate hydrogen and increase the rate of hydrogenation relative to hydrogenolysis which would produce ethene.[38]

Dissolution of Fe and B. For Fe(B) in argon, ∼25% of the boron in the particles was released after 5.5 h, increasing to 70% after 2 days (Figure 5a). Greater than 90% of total mass of boron in the Fe(B) was released into solution by the end of the reaction. Release of iron (∼95% is Fe(II)) into the solution coincided with the release of boron; however, only 35% of the total Fe^0 added was present as dissolved Fe. The complete release of boron from the particles and the complete accessibility of Fe^0 suggest that the particles are dissolving during reaction with TCE. The apparent lack of complete dissolution of Fe^0 to dissolved Fe(II) may be a result of dissolved iron precipitating from solution as an iron oxide or hydroxide. Iron precipitation is consistent with HRTEM images taken of precipitated particles after 23 days of reaction which show that they are euhedral and crystalline (Figure S1). Particle dissolution and precipitation was also speculated by Nurmi et al. by observing similar particles after reaction.[11] With added H_2, the release of boron and iron from the particles showed a similar trend, but the release occurred in a shorter time (∼1 day) as did the TCE dechlorination reaction (Figure S2). The

(38) Arnold, W. A.; Roberts, A. L. *Environ. Sci. Technol.* **2000**, *34*, 1794−1805.

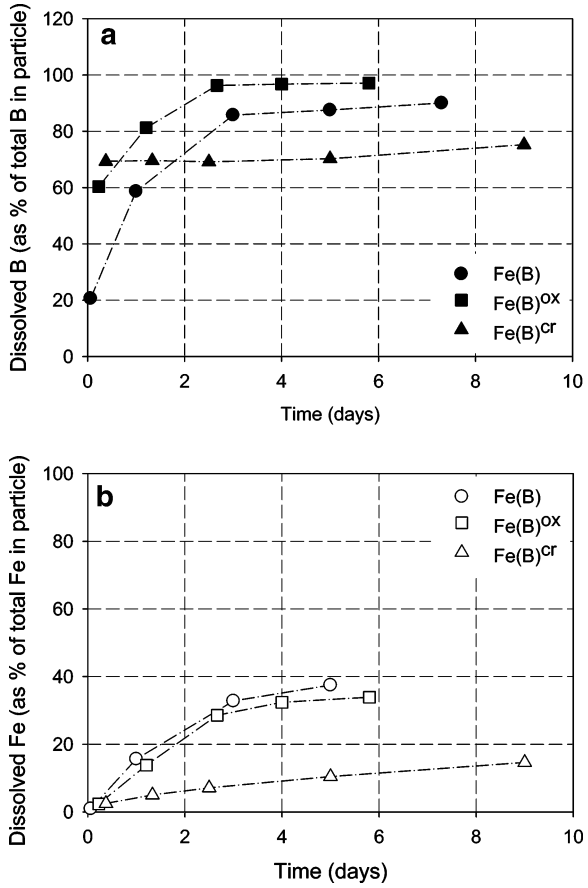

Figure 5. Dissolved Fe and B for reactions in an Ar headspace with 40 mg of particles and 2.2 mM TCE: (a) dissolved B; (b) dissolved Fe.

high correlation between the rate of TCE reaction and the rate of iron and boron dissolution again suggests oxidative dissolution of the particles by TCE.

Effect of Partial Oxidation. Partially oxidized particles had a slightly longer period of slowed reactivity (15−20 h) compared to fresh particles, but partial oxidation did not significantly affect the steady maximum Fe^0-normalized reaction rate (Figure 3a), the reaction product distribution (Table 3), the H_2 utilization pattern (Figure 4b), or the ability to activate and use H_2 for TCE reduction (Figures 4b and 3a). The rate of release of iron and boron from particles during reaction is also relatively unaffected by partial oxidation (Figure 5). For $Fe(B)^{ox}$ the initial release of boron was higher than for Fe(B) but showed a similar trend for release during reaction; i.e., release of B and Fe were concomitant with the TCE reaction.

Effect of Annealing. Annealing and subsequent crystallization of the nanoiron had a significant effect. The lag phase observed for Fe(B) and $Fe(B)^{ox}$ did not occur with $Fe(B)^{cr}$, despite the HRTEM-observable "shell" on the particles (Figure 1c). This suggests that the TEM-observable shell is not responsible for the lag phase. Without the lag phase, TCE loss and subsequent product formation for $Fe(B)^{cr}$ displayed typical pseudo-first-order kinetics with slow deactivation (Figure 3b). The TCE dechlorination reaction slowed over time, and after 40 days the reactions became too slow to measure. The surface area normalized first-order reaction rate constant was $(1.2 \pm 0.2) \times 10^{-3}$ $L \cdot h^{-1} \cdot m^{-2}$ under both argon and H_2 headspace. Good model fits were only achieved when first-order deactivation was considered ($k_d = 0.17 \pm 0.03$ d^{-1}). For $Fe(B)^{cr}$, reaction products were predominantly unsaturated, with acetylene (81−83%) and ethene (11−14%) accounting for nearly all of the dechlorination products (Table 3).

With or without TCE present, little H_2 was evolved from $Fe(B)^{cr}$ compared to Fe(B) and $Fe(B)^{ox}$ (Figure 4), indicating a lower reactivity with H_2O. Adding H_2 to the headspace did not increase the TCE dechlorination rate or alter the observed products from $Fe(B)^{cr}$. The unresponsiveness to H_2, and the unsaturated products formed indicate the inability of $Fe(B)^{cr}$ to activate and use H_2. The lack of activated hydrogen decreases the rate and extent of the hydrogenation, leading to fewer saturated products. A similar product distribution was observed for RNIP particles which were also crystalline and unable to activate and use H_2 for TCE dechlorination.[10] In both cases (argon or H_2 headspace), after 18 days the TCE reaction products accounted for only 50% of the Fe^0 (electrons) initially in the particles. Particles removed from the reactor after 23 days contained 40% of the Fe^0 that was initially in the particles, and after 105 days ~15% of the Fe^0 remained in the particles. The relative inaccessibility of Fe^0 in $Fe(B)^{cr}$ is markedly different than with Fe(B) and $Fe(B)^{ox}$, indicating that annealing and subsequent crystallization made a large fraction of the Fe^0 less readily available for reaction.

Annealing and crystallization also affected the release of boron from the particles. Approximately 60−70% of the total boron initially present in $Fe(B)^{cr}$ was released in only 1.5 h (Figure 5a). This release also occurred in the absence of TCE (not shown) and is consistent with the higher concentration of boron on the particle surface observed by XPS. After the rapid initial release a more gradual release of boron was observed (~6%) during reaction with TCE over 18 days, and not all of the boron in the particles was released. The gradual and incomplete release of boron corresponds with the lower reactivity of $Fe(B)^{cr}$ and the incomplete accessibility of the Fe^0. As with Fe(B) and $Fe(B)^{ox}$, the dissolved iron concentration steadily increased during the reaction and stopped at ~25% of the total Fe^0 added to the reactor. The release of dissolved boron and iron was coincident with TCE dechlorination, and identical trends were observed in both H_2 and argon headspace.

Important Factors Controlling the Reactivity of Nanoiron Produced from Borohydride Synthesis. Nanoiron made from borohydride reduction of dissolved iron has been shown to have unique features compared to granular iron or to other types of nanoiron, including the ability to dechlorinate PCBs at ambient temperature and pressure,[8] approximately a 4-fold higher surface area-normalized TCE dechlorination rate constant than for another nanoscale iron,[10] and lengthy equilibrium time in Tafel measurements.[13] The TCE degradation rate and reaction products formed by this nanoiron are strongly influenced by the degree of crystallinity of the material. The highly disordered nature of Fe(B) and $Fe(B)^{ox}$ provides them the ability to activate and use H_2, which increases the rate and extent of hydrogenation and yields more saturated reaction products compared to crystalline Fe^0, e.g. $Fe(B)^{cr}$, RNIP, and iron filings. The presence

of boron appears to be a less important feature than the degree of crystallinity because crystalline particles ($Fe(B)^{cr}$) containing ~2 wt % (~9 at. %) boron could not activate H_2 while highly disordered particles (Fe(B) and $Fe(B)^{ox}$) containing <1 wt % boron (~5 at. %) after 2.5 days reaction (Figure 5a) continued to activate and use H_2 as evidenced by the continual decrease in H_2 headspace concentration (Figure 4b). Further, the features of TCE dechlorination by $Fe(B)^{cr}$, i.e., surface area normalized reaction rate constant, the TCE reaction products formed, and the inability to access all of the Fe^0 are similar to those of RNIP.[10] The physicochemical property that these two types of nanoiron particles share is their crystalline α-Fe^0 structure so it is likely that the degree of crystallinity of nanoiron is a more important factor controlling their reactivity than the presence or absence of boron.

Oxidative dissolution of Fe(B) and $Fe(B)^{ox}$ can explain the complete access to Fe^0 and the complete release of boron incorporated in these particles, as well as the crystalline precipitate observed in the reaction with TCE. Nanoiron dissolution during TCE reduction would continually change the active surface area available for reaction and suggests that normalizing the reaction rate constants by the particle surface area, a commonly used method for comparing reaction rates for different forms of Fe^0, may not be appropriate for nanoiron synthesized by borohydride reduction of dissolved Fe(II).

Conclusions

Fresh (Fe(B)), partially oxidized ($Fe(B)^{ox}$), and annealed ($Fe(B)^{cr}$) nanoiron synthesized from aqueous borohydride reduction of dissolved Fe(II) was studied. Fe(B) and $Fe(B)^{ox}$ are poorly ordered materials and can activate and use externally supplied H_2 for TCE hydrodechlorination. The hydrodechlorination reaction pathway increases the rate of TCE dechlorination and leads to more saturated products (e.g. ethane) than observed for iron filings or for other types of crystalline nanoiron. Annealing and subsequent crystallization of the nanoiron took away the ability to activate H_2, decreased the TCE dechlorination rate to that observed for iron filings and crystalline nanoiron, and produced mostly unsaturated products. Differences in nanoiron reactivity are attributed to the particle morphology, i.e., the amorphous or short-range order atomic structure of Fe(B) and $Fe(B)^{ox}$ vs the crystalline structure of $Fe(B)^{cr}$, rather than the presence or absence of boron. The TEM-observable shell on the particles does not correlate with the reactivity of the particles in water. Fe(B) and $Fe(B)^{ox}$ undergo oxidative dissolution during reaction, making all of the Fe^0 accessible for reaction. Particle dissolution suggests that a core−shell model for amorphous Fe(B) may be inaccurate and that normalizing the observed reaction rate constants to particle surface area for comparison with other types of Fe^0 may not be appropriate.

Acknowledgment. This research was funded in part by the Office of Science (BER), U.S. Department of Energy, Grant No. DE-FG07-02ER63507, and in part by the U.S. EPA (Grant R830898). Although the research described in this paper has been funded by the U.S. Environmental Protection Agency, it has not been subjected to the Agency's required peer and policy review and therefore does not necessarily reflect the views of the Agency, and no official endorsement should be inferred. Any opinions, findings, and conclusions or recommendations expressed in this material are those of the authors and do not necessarily reflect the views of the Department of Energy. The authors thank the EMSP project team at CMU for insightful and helpful discussions. The authors also thank Madhur Sachan (Carnegie Mellon University) for reducing the particles and Prof. Greg Rohrer for the use of his GC/TCD.

Supporting Information Available: HRTEM images and SAED of Fe(B) and $Fe(B)^{cr}$ after reaction (Figure S1) and the dissolved Fe and B concentrations in the reaction solution with H_2 headspace (Figure S2) (PDF). This material is available free of charge via the Internet at http://pubs.acs.org.

CM0511217